Book of Tutorials and Abstracts

European
Microbeam Analysis Society

University of BRISTOL

Mineralogical Society

EMAS 2018

13th EMAS Regional Workshop

MICROBEAM ANALYSIS IN THE EARTH SCIENCES

4 - 7 September 2018

University of Bristol, Wills Hall, Bristol, Great Britain

Organised in collaboration with:
Mineralogical Society of Great Britain and Ireland
and
University of Bristol

QUANTITATIVE CHEMICAL ANALYSIS OF DIAMOND ANVIL CELL EXPERIMENTS AND OTHER TINY SAMPLES

E.S. Jennings[1,2] and J. Wade[3]

1 University of London, Birbeck, Department of Earth and Planetary Sciences
Malet Street, London WC1E 7HX, Great Britain
2 University of Bayreuth, Bayerisches Geoinstitut
95440 Bayreuth, Germany
3 University of Oxford, Department of Earth Sciences
South Parks Road, Oxford OX1 3AN, Great Britain
e-mail: e.jennings@bbk.ac.uk

Eleanor Jennings is a lecturer at Birkbeck, University of London. She received a MSci in Geology from the University of Bristol in 2010, where she then worked as a laboratory technician for a year. She completed her PhD at the University of Cambridge in 2015, before working as a postdoctoral researcher at the University of Bayreuth, performed diamond anvil cell experiments (amongst others): this required quatitative analysis of the µm-sized run products and their nm-sized textural features, and drove her to examine the limitations of the EPMA technique for analysing such samples.

ABSTRACT

There are many techniques available to make site-specific quantitative chemical analyses of tiny samples, i.e., samples on the order of 1 - 10s of micrometres (which may themselves contain even tinier heterogeneities). Specifically, we are considering the analysis of the products of diamond anvil cell (DAC) experiments, although the limitations will be much the same for any other tiny, heterogeneous geologically-relevant sample. Measurements of larger samples such as thin sections may also occasionally require a high spatial resolution for detailed microtextural examination. We begin by listing and briefly describing many techniques that can, and have, been used for examining such samples. Following this, the case of using EPMA for tiny samples is examined in more detail by quantifying the effects of sample thickness and secondary fluorescence using both simulations and measurements of synthetic samples. Quenched molten metal from DAC experiments often contains a sub-μm exsolution texture: we explore the composition of the exsolved phase and the nature of the interface with the matrix by atom probe tomography (APT), and discuss its implications for 'large' spot EPMA measurements of these quenched metals.

1. QUANTITATIVE ANALYTICAL TECHNIQUES FOR TINY SAMPLES

1.1. Analytical techniques

1.1.1. Electron probe microanalyser (EPMA). EPMA is by far the most commonly used technique to measure chemical composition in Earth sciences, and is discussed elsewhere in this workshop. It offers rapid, fully quantified analyses at micron-scale spatial resolutions, combined with low relative errors (< 2 %). For EPMA measurement, a flat polished surface is required, which is traditionally achieved by mechanical polishing. However, because of the awkwardly small dimensions of diamond anvil cell (DAC) samples – typically less than 100 μm in diameter and less than 10 μm thick – a polished surface is more usually achieved through physical extraction of the analytical area and milling using a focussed ion beam (FIB).

Although EPMA is considered a routine technique, it was not originally envisaged for very small samples. Users are too frequently unaware of the limitations of EPMA for tiny samples, because the limitations of the technique are not something that are usually considered relevant when measuring crystals of 100s μm or more in a thin section. Difficulties stem from the fact that although the beam can be focussed to a sub-μm diameter on a sample surface, electrons and X-rays are able to travel and spread within the sample. The volume within which electrons can travel, interact with atoms and excite X-rays (and so generate a primary signal), the "interaction volume", is ~1 μm diameter at typical operating conditions of 15 to 20 kV. Worse, X-rays themselves can excite secondary X-rays, and given that high energy X-rays are less impeded than electrons and can travel much further in a material, the generation of signal from 10s - 100s μm from the analytical point represents a minor, but potentially important, source of contamination and

analytical error. When we talk about tiny samples, thin samples, or measurements made very close to grain boundaries, such as when analysing high pressure experimental samples, these represent the limitation of the technique (further explored in section 2).

There are many examples in the literature of EPMA used for the measurement of DAC samples. These include partitioning studies, where two or more phases are equilibrated at temperature, quenched, and analysed [1-6], with many studies focused on planetary core formation. These experiments usually involve equilibration of metals with silicates at very high pressures (in excess of 300,000 atm) and temperatures (3,000+ K). The extreme heterogeneous nature of these experiments, coupled with their small size, present the worst of all worlds for the analyst. We detail here how to minimise both wasted effort, and also methods to reassess published data.

It should also be noted that an EPMA equipped with a field emission gun rather than a filament may be more appropriate for the measurement of tiny samples, as the beam can be better focussed at low accelerating voltages, reducing the interaction volume. For example, Tateno *et al.* [7] measured the composition of quenched melt phases in DAC melting experiments performed at lower mantle conditions using a 10 kV_{acc} beam, and Sinmyo and Hirose [8] mapped Soret diffusion in a DAC using this method, also at 10 kV_{acc}. However, whilst this offers benefits in spatial resolution, it presents difficulty with measuring higher energy characteristic X-rays such as Fe-Kα_1. Furthermore, instrumental effects such as carbon deposition must also be minimised for analysis to be meaningful.

Finally, energy-dispersive X-ray spectrometry (EDS) measurements have also been used for measuring DAC experiments, on an SEM or EPMA instrument. For example, Chidester *et al.* [9] measured DAC experiments examining the high P-T metal-silicate partitioning of U by EDS. However, spectral resolution and detection limits are significantly better in WDS than EDS, so WDS is preferred for fully quantitative analyses. EDS is convenient and a useful tool for elemental mapping and, when fully calibrated, can be very useful for analysing major elements, leaving WDS spectrometers to measure the minor and trace element components.

1.1.2. Transmission electron microscope (TEM). TEM involves transmitting a focussed beam of electrons through a thin sample, and the possible range of modes of use and types of analyses are dictated by the instrumentation. Spatial resolution is much higher than in an SEM (also EPMA), allowing (for example) crystallographic defects to be imaged, and crystallographic data can be obtained by electron diffraction. A very high accelerating voltage is frequently used relative to SEM/EPMA to give a higher resolution, since it is assumed that electron scattering is negligible during the beams journey through the sample.

A particular adaptation of TEM, STEM (scanning TEM), involves rastering the finely-focussed beam over the sample. When combined with an analytical TEM technique (e.g., EDS, electron energy loss spectroscopy (EELS)), this can be used to obtain elemental and/or chemical maps of a

sample. As with SEM/EPMA, a spectrum of emitted characteristic X-rays can be measured by an EDS detector: this can be used to obtain either point analyses or maps of relative elemental concentrations of a sample at a nm-scale spatial resolution. Measurement is usually standardless and requires knowledge of *k*-factors and sample thickness to calibrate the counts. EELS relies on the fact that primary electrons that pass through the sample will lose some energy through inelastic scattering interactions with electrons from within the sample. This technique is complementary to EDS, but is more sensitive to lower atomic number elements. Both of these techniques give better spatial resolution, but worse precision and accuracy, than WDS by EPMA, and may also be affected by fluorescence artefacts as discussed for EPMA in section 1.1.1.

In order to be analysed by TEM, samples must be electron-transparent (e.g., ~100s nm thick, material- and accelerating voltage-dependent). Geological samples can be prepared by FIB or by ion milling (e.g., [10, 11]). Sample preparation for TEM is generally more difficult and time-consuming than for EPMA/SEM.

STEM with EDS and EELS has long been used to measure elemental concentrations in many tiny natural geological samples and DAC experiments. Frost et al. [12] analysed DAC experiments to examine O partitioning between quenched liquid iron veins and solid magnesiowüstite. Fischer *et al.* [13] analysed quenched liquid metal – liquid silicate DAC partitioning experiments using a broader spot size of 0.5 - 2 μm (to integrate fine quench textures). In both cases, STEM was used, with relative elemental concentrations determined by standardless EDS, and relative O ± C concentrations determined by EELS.

1.1.3. Synchrotron micro-X-ray fluorescence (SR-μXRF). XRF has similarities to EPMA, but the fluorescence of characteristic X-rays from a material is induced by irradiation with high-energy primary X-rays rather than electrons. This is a commonly-used technique in a range of fields for larger samples. In μXRF, the X-ray beam is focussed to a small spot. Synchrotron radiation (SR) provides the high X-ray flux typically required for the high spatial resolution and sensitivity needed to measure tiny samples. Detection limits can be lower and spot sizes smaller than for EPMA analysis.

Unlike electron microbeam techniques, high-energy X-rays can penetrate significant depths through various materials. Therefore, one benefit of SR-μXRF is the possibility of measuring DAC experiments through diamond, meaning that high pressures and/or temperatures can be applied, and fluids can be measured *in-situ* [14, 15] without quenching. However, some difficulties with this technique. Matrix corrections must be made for X-ray absorption by the sample, and secondary effects occur such as the absorption of fluoresced X-rays and subsequent emission of additional secondary X-rays (known as enhancement). The volume from which X-rays can be generated through enhancement is potentially much larger than the focussed beam spot size. This should be considered in the context of measuring tiny samples and measuring close to interfaces. Additionally, the interaction volume for each X-ray is dependent on its characteristic energy: this

makes the resolution of an XRF map dependent on the energy of the X-ray, and makes matrix corrections difficult, since the effective interaction volume changes with characteristic X-ray energy.

SR-μXRF has been used for the in-situ measurement of many tiny geologically-relevant samples in DAC experiments where there is a requirement to physically retain a fluid phase at high-PT conditions, e.g., mineral solubility studies [14, 16]. Andrault *et al.* [17] used SR-μXRF to make elemental maps with ~1 μm spatial resolution of a quenched DAC experiment to examine partitioning of FeO between solid phases and liquid at lower mantle conditions. SR-μXRF has also been pioneered in the analysis of quenched liquid metal – liquid silicate DAC partitioning experiments, where detection limits of 2 - 5 ppm allow the analysis of strongly siderophile or lithophile elements which are trace elements in one phase [18].

1.1.4. Atom probe tomography (APT). APT is a powerful technique, allowing the identification and 3D mapping of individual atoms in a sample (reviewed elsewhere e.g., [19]). However, it is also amongst the most difficult, expensive and time-consuming techniques in terms of sample preparation and analytical success. It is best suited to one-off measurements, and is more successful for conductive materials, which better withstand the analytical conditions. Samples are on the order of 100s nm and features at the sub-nm (atomic) scale are resolvable, so this is best suited for when extremely high spatial resolution is required. A sample must be prepared as a sharp needle tip. The evaporated atoms are ionised and identifiable by their mass/charge ratio (i.e., isotopic identification is possible). Detection efficiency is very high, and using the position and relative timing of counts, a 3D image is reconstructed.

APT is not routinely used in the Earth sciences because insulating materials are not best suited to the high field gradients. It has, however, occasionally been applied to natural samples where nm-scale 3D resolution and compositional identification are required. Some notable examples include: *i*) characterising Pb nanoclusters within Earth's oldest zircon [20]; *ii*) the U-Pb dating of impact and crystallisation events from discrete nanostructural domains in baddeleyite [21]; *iii*) developments in APT that are being made towards the characterisation of the C isotopic composition of pre-solar nanodiamonds (e.g., [22]). In section 3.2, we present APT measurements of exsolution within quenched metal from a DAC experiment.

1.1.5. Nanoscale secondary ion mass spectrometry (nanoSIMS). SIMS relies on a primary ion beam (e.g., O^- or Cs^+) that bombards the sample and sputters ionised material; these secondary ions are analysed by a mass spectrometer. It can be effective for both chemical mapping and spot analyses. NanoSIMS is a variant of SIMS optimised for nanoscopic scale spatial resolution, with theoretical resolutions of ~35 nm. Like SIMS, it has the advantage of making isotopic as well as elemental measurements. However, using a very small spot size compromises on analytical sensitivity. SIMS techniques depend on appropriate standardisation, as the ionisation efficiency of various elements is matrix-dependent, so closely matrix-matched standards are needed to convert

counts to composition. In nanoSIMS, even variations in surface topography and sample morphology can cause offset relative to standards: analyses have a reputation for being difficult. SIMS/nanoSIMS require a highly polished surface for analysis.

NanoSIMS is a well-known technique for tiny samples, and is particularly used for its isotopic analysis capability. For example, it is used is cosmochemical studies of extra-terrestrial materials such as presolar grains [23]. NanoSIMS has also been used in the chemical analysis of DAC experiments when a high spatial resolution or light element measurement is required [24]); recently, Suer *et al.* [25] quantified the S content of run products in DAC metal-silicate partitioning experiments. However, the trade-off between sensitivity and analytical resolution is ever-present whilst matrix matching of exotic materials, and in particular metals derived from very high pressure experiments, is not trivial.

1.2. Focussed ion beam sample preparation for EPMA, TEM and APT

Most commonly, DAC experiments are prepared for EPMA analysis by FIB. Unlike conventional polishing, this gives fine control over the sample site and shows 3D context (for example, the lamella can be imaged front and back). For EPMA analysis, a lamella of at least several μm thickness is required – this can be subsequently thinned further for TEM analysis. The complete process is shown in Fig. 1, using a DAC experiment with a molten metal sampling region as an example. A dual-beam instrument allows imaging with an electron beam and milling with a Ga^+ beam. Firstly, the site is identified at the top of the gasket chamber. A strip of Pt is deposited as a marker and to protect the sample top from beam damage. A trench is then milled out on either side using a high energy Ga^+ beam and the sample is thinned to several μm thickness with successively lower currents (for better focussing and to protect from beam damage and Ga^+ implantation). The lamella is then welded to a manipulator (W needle) using Pt, is cut free from the sides, and is lifted out. Following this, the lamella is welded to a Cu sample holder post, cut free from the manipulator, thinned to the final thickness, and cleaned of implanted Ga^+ and redeposited material by rastering a successively lower current and voltage Ga^+ beam. For TEM analysis, these final stages must be carefully performed to produce an electron-transparent sample.

A related procedure can be used to produce an ATP needle tip: 1) a wedge-shaped ('toblerone') chunk is cut from a sample, welded to the manipulator using Pt, cut free and lifted out; 2) the end of this chunk is welded to a truncated Si needle (a post) of a sample holder and cut free from the manipulator; 3) the sample holder is tilted such that the needle is parallel to the beam; 4) the beam is rastered over a ring-shaped area, that becomes successively smaller and lower current/voltage, until an extremely low power beam is used for the final sharpening to a ~ 30 nm point. A very low power beam is required to remove traces of Ga^+ implantation.

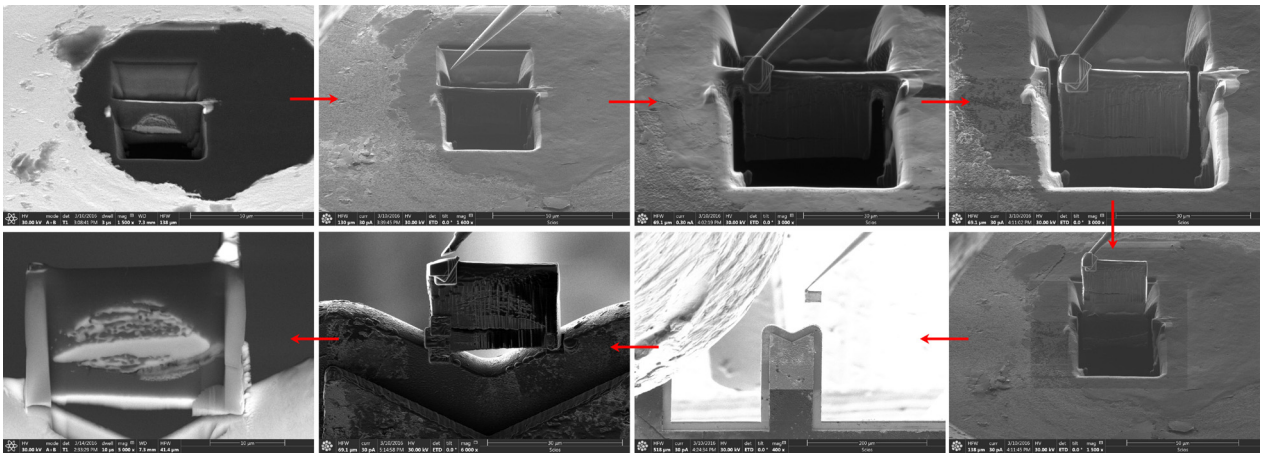

Figure 1. The process of preparing a sample as a lamella for EPMA or TEM by FIB.

2. *USING EPMA TO ANALYSE DAC EXPERIMENTS AND OTHER TINY SAMPLES: SOME CONSIDERATIONS*

In this section we explore the limitations of EPMA measurements of tiny samples by using both Monte Carlo simulations and by making real EPMA measurements of synthetic samples. We focus here on iron alloys, basaltic glass, and the interface between the two. These phases have strongly contrasting properties and compositions, highlighting the general difficulties in measuring small samples with chemically contrasting phases. The principles and methods are applicable to any similar situation.

2.1. Methods

2.1.1. EPMA measurements. Analyses were performed using a JEOL JXA 8200 EPMA at the University of Bayreuth with a 15 kV_{acc}, 15 nA focussed beam for metals, and a 1 μm diameter beam for silicate glasses. Typical thick polished standards appropriate to the material were chosen. Measured lines for most elements were $K\alpha_1$. $L\alpha_1$ was used for Mo. W was measured using $L\alpha_1$ with long counting times. The default JEOL $\Phi(\rho z)$ correction (metal: XPP [26]; oxide: [27, 28]) was applied.

2.1.2. Simulations. Fully quantified Monte Carlo simulations of the EPMA analyses were performed using the simulation package PENEPMA (v. 2014) [29, 30]. PENEPMA simulates the geometry of a typical EPMA analysis, in addition to the electron transport and resultant X-ray generation within electron-irradiated materials. It uses the general-purpose PENELOPE code [31] optimised for EPMA-type applications. The high degree of accuracy of such Monte Carlo simulations has been previously demonstrated by comparing simulations with EPMA measurements for a range of materials (e.g., [26]).

Although PENEPMA can be used to simulate the detector geometry of an EPMA (spectrometer positions and window sizes), such a realistic simulation is not feasible due to the extremely low count efficiency and thus extremely long calculation times. As a compromise, we follow the approach of Wade and Wood [32] and use an annular (360°) detector with a 35 - 45° vertical extent (Fig. 2). This assumes that X-ray trajectories will have randomly distributed horizontal components, which is not strictly true of samples with a planar boundary.

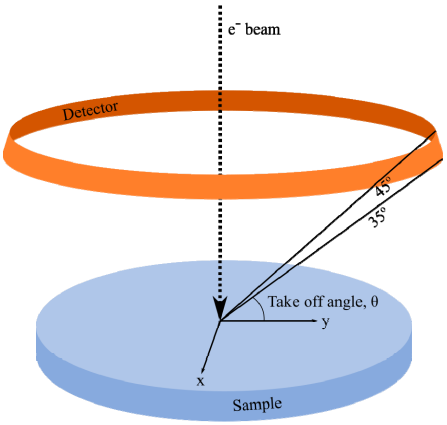

Figure 2. Annular detector setup used in simulations, after Wade and Wood (2012).

K-ratios (the ratio of counts from unknowns to counts of standards) were determined by simulating large standards, infinitely thick with respect to the electron beam, of the same composition as the materials of interest, with the same conditions and detector. The default Armstrong/Love Scott $\Phi(\rho z)$ correction was applied using CalcZAF [33] to convert *k*-ratios to concentrations, mimicking EPMA data treatment.

2.2. Sample thickness

2.2.1. Background. A sample with small x and y dimensions is probably also thin in the third dimension. DAC experiments may be just 10 µm thick, and once the heated region of interest is extracted and prepared by FIB, it may be just a few µm thick. DAC metal–silicate partitioning experiments are usually prepared as lamellae that are 1 - 4 µm thick. Thin samples give low counts relative to a thick standard. If the primary electron volume is truncated, then electrons will be lost through the sample base, resulting in a significant reduction in generated X-rays. Even if the sample is thicker than this primary interaction volume (Fig. 3), high-energy photons, which will penetrate further than electrons, will be lost from the base and result in lower measured counts from secondary fluorescence. These normally contribute a small fraction of the signal in a 'thick' sample. These effects can be mitigated by calibrating with thin standards, although this represents a huge additional workload and expense, and it is unlikely that standards and samples will be manufactured to identical thicknesses. Alternatively, a thin film correction procedure could be used.

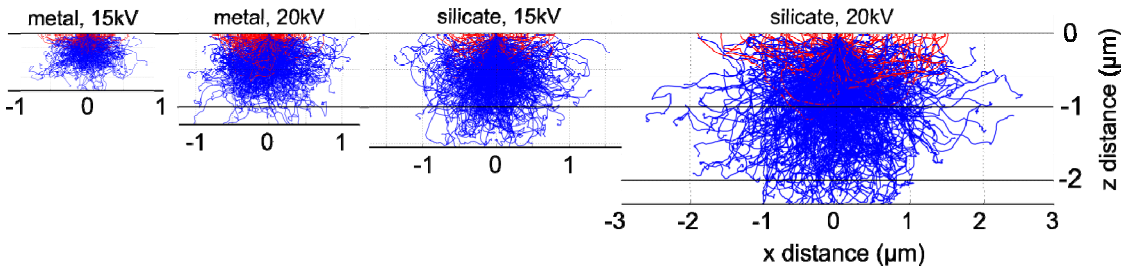

Figure 3. Primary electron interaction volumes (projected to 2D) for different materials and voltages. Red are backscattered electrons; blue are electrons absorbed by the sample.

We have determined practical thickness limits for a) iron alloys ($Fe_{85}Ni_5Mo_5W_5$, wt.%), and b) synthetic CFMAS basaltic glass (13.0 wt% MgO, 22.4 wt% Al_2O_3, 46.4 wt% SiO_2, 11.2 wt% CaO, 5.1 wt% Fe_2O_3), using both simulations of different thicknesses in PENEPMA, and by making EPMA measurements of wedges cut from the synthetic glass and alloy. Wedge-shaped samples with dimensions similar to DAC sample lamellae (10 x 20 x 1 - 3 µm) were cut by FIB and welded to Cu TEM sample holders using Pt deposition (Fig. 4).

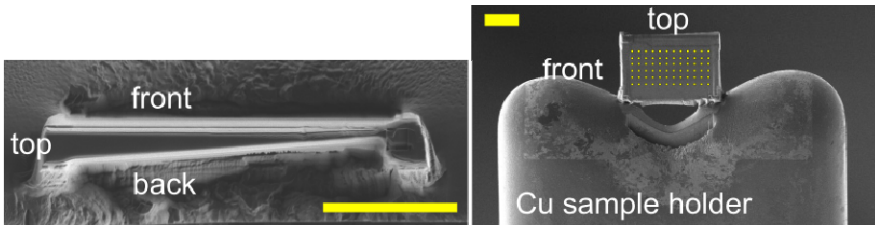

Figure 4. Primary electron interaction volumes (projected to 2D) for different materials and voltages. Red are backscattered electrons; blue are electrons absorbed by the sample.

2.2.2. Results. Measurements and simulations across the $Fe_{85}Ni_5Mo_5W_5$ metal wedge are shown in Figs. 5a and 5b. From 900 to 2,300 nm, there is no clear change in elemental concentrations measured by EPMA, which is in good agreement with the simulations. In the simulations, apparent concentrations sum to around 99.6 % at 4,000 nm and decrease as the sample thins, although a strong drop-off is only observed when the metal is thinner than 500 nm, which reflects a truncation of the primary interaction volume. In pure Fe, the depth over which 95 % of interactions occur reaches a maximum of ~530 nm; electrons are lost from the base of samples thinner than this, leading to a difference in the interaction volumes between the thick standards and the thinned sample. Figure 5c shows the simulated apparent concentrations as a proportion of the thick standard. Where the primary interaction volume is truncated (e.g., in the 250 nm simulation), the intensities of the various X-ray lines are unequally diminished, with the higher energy X-ray lines apparently reduced to a greater extent. This results in erroneous measured elemental ratios, and implies that measurements of thin samples cannot be easily normalised to 100 % without

introducing non-systematic errors. Fe-rich alloys can be analysed with an accelerating voltage of 15 kV_{acc} to a thickness of around 1000 nm without introducing significant analytical errors. TEM wafers, typically of approximately 200 nm thickness, require appropriate standards of the same thickness if they are to be analysed by EPMA, or a thin film correction must be applied.

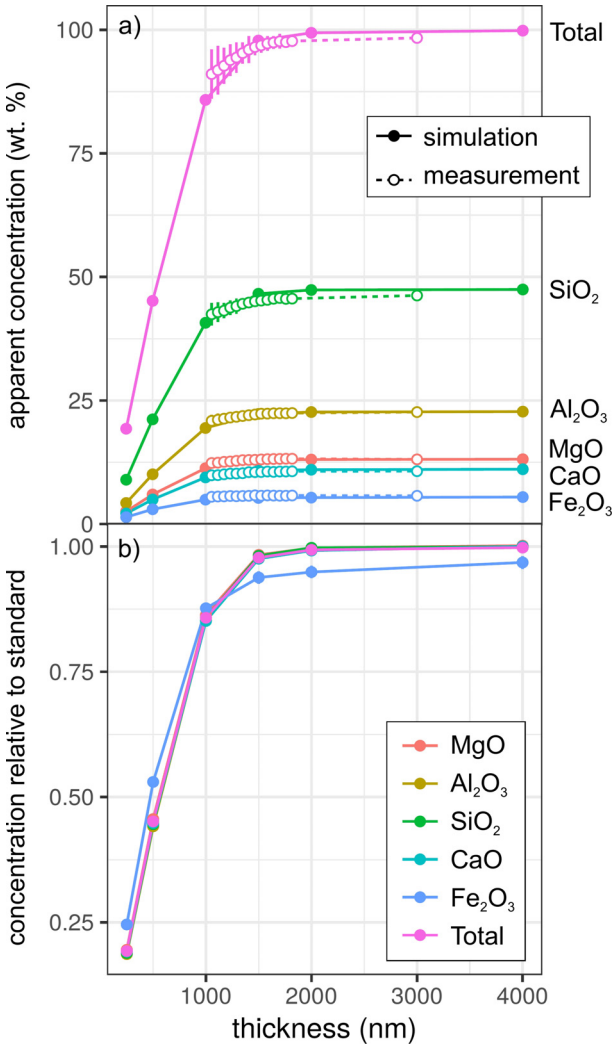

Figure 5. Simulations and EPMA measurements along a synthetic CFMAS basaltic glass wedge, showing apparent concentration as a function of thickness. Symbols as for Fig. 6. a) Apparent concentration of all oxides and total; b) simulated concentrations divided by those from a simulated thick standard.

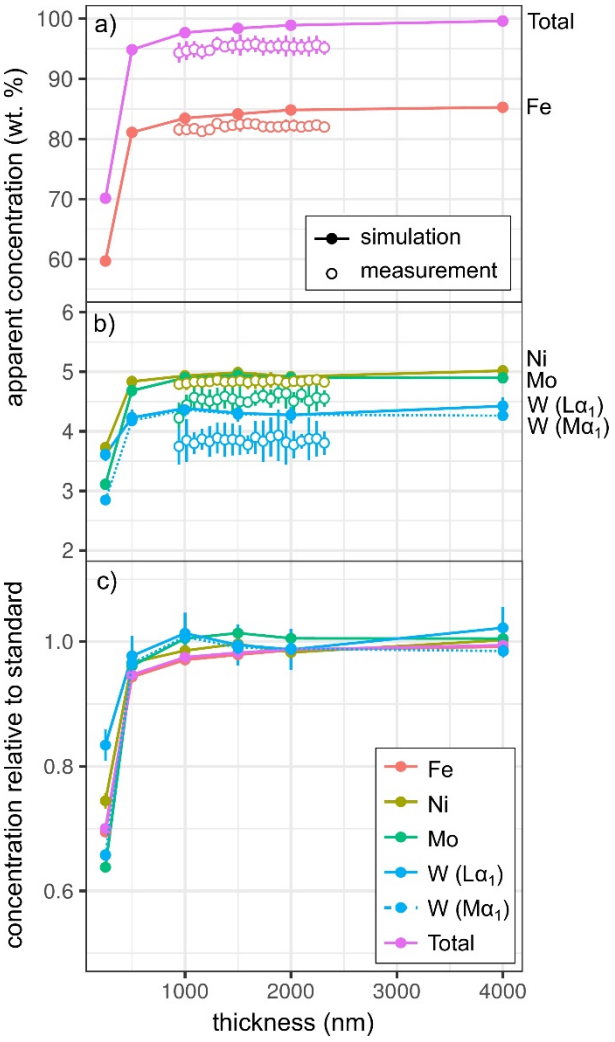

Figure 1. Simulations and EPMA measurements along a metal $Fe_{85}Ni_5Mo_5W_5$ wedge, showing apparent concentration as a function of thickness. Open symbols are measurements, closed are simulated points. 2σ uncertainties. a) Fe and total wt %; b) Ni, Mo and W (note change in scale); c) simulated concentrations divided by their concentration in a simulated thick standard.

Results for the synthetic basalt wedge measurement and simulation are shown in Fig. 6. The effect of reduced thickness on the apparent concentrations is more pronounced than for the metal: X-ray production reduces noticeably at 1,500 - 2,000 nm in both simulation and EPMA measurement. This results from the lower density of the basalt (~3 g cm^{-3}) in comparison to the metallic sample (7.8 g cm^{-3}), and hence the lower electron stopping power and the larger resultant interaction volume. The drop-off in X-ray intensity is significant: at < 1,500 nm, silicate samples are not analysable with any degree of confidence using standard analytical routines. However, unlike in the metal sample, ratios of oxides are approximately preserved (Fig. 6b), except for iron (because most of the silicate-forming elements have similar interaction volumes). Absolute concentrations in thin silicates will be erroneous, and whether or not a composition can be normalised to 100 % depends on the particular elements present. The consistency of the EPMA measurements with the simulations in Fig. 6 demonstrates that simulations are an effective method to test for the presence of thickness-related analytical problems when working with FIB-prepared DAC experiments and other small samples.

2.3. Fluorescence across an interface

2.3.1. Background. High energy X-rays are less attenuated than electrons, and so secondary fluoresced X-rays generated by excitation both from by primary and continuum X-rays possessing energies above the critical excitation edge can be generated at significant distances (tens of μm) from the point of analysis [35]. This can generate a spurious signal from nearby materials, causing artefacts in the data. Fluorescence profiles may appear like, or enhance, diffusion profiles [35]. When measuring an element which is in trace concentration in one phase and is in major concentration in an adjacent phase, secondary fluorescence can lead to an overestimation of the trace concentration, which will reduce the apparent concentration contrast and shift ratios towards 1:1, with implications for partitioning studies [32, 36]. This is of particular concern in very small samples, as it will be difficult to place the analytical spot far enough away from an interface to mitigate for this. Significant secondary fluorescence from a neighbouring phase can be detected tens of μm from an interface [32, 36], which is problematic in the analysis of multi-phase DAC experiments, or measuring small crystals in larger samples.

Wade and Wood [32] investigated fluorescence of Ni in DAC metal-silicate partitioning experiments through simulations. They identified large and unavoidable fluorescence contributions, and recommended that future workers use simulations to investigate potential analytical artefacts and potentially apply corrections to their data. We extend this by using simulations and measurements of samples, to identify the extent to which different elements are affected. We apply this approach to sections removed from DAC experiments by FIB methods.

We created a mechanically pressed interface (synthetic grain boundary) to examine fluorescence between pure forsterite and pure iron. The two materials, with a straight interface between them and confined in a gasket, were pressed together in a DAC without heating, ensuring no reaction

between the coexisting phases. The gasket was then mounted and polished to expose the boundary without surrounding topography, and a low-angle transect was analysed across it by EPMA. The same experiment was simulated in PENEPMA. In addition, an interface between forsterite and an Fe alloy ($Fe_{15}CrCoNiMoW$) was simulated.

2.3.2. Results: the metal-silicate interface. The apparent concentrations from measurements and simulations across a planar interface between forsterite and iron are shown in Fig. 7, and the spatial distribution of the origin of secondary fluoresced X-rays is shown in Fig. 8. The measurements and simulations closely match one another, in agreement with previous comparative studies [30 and references therein].

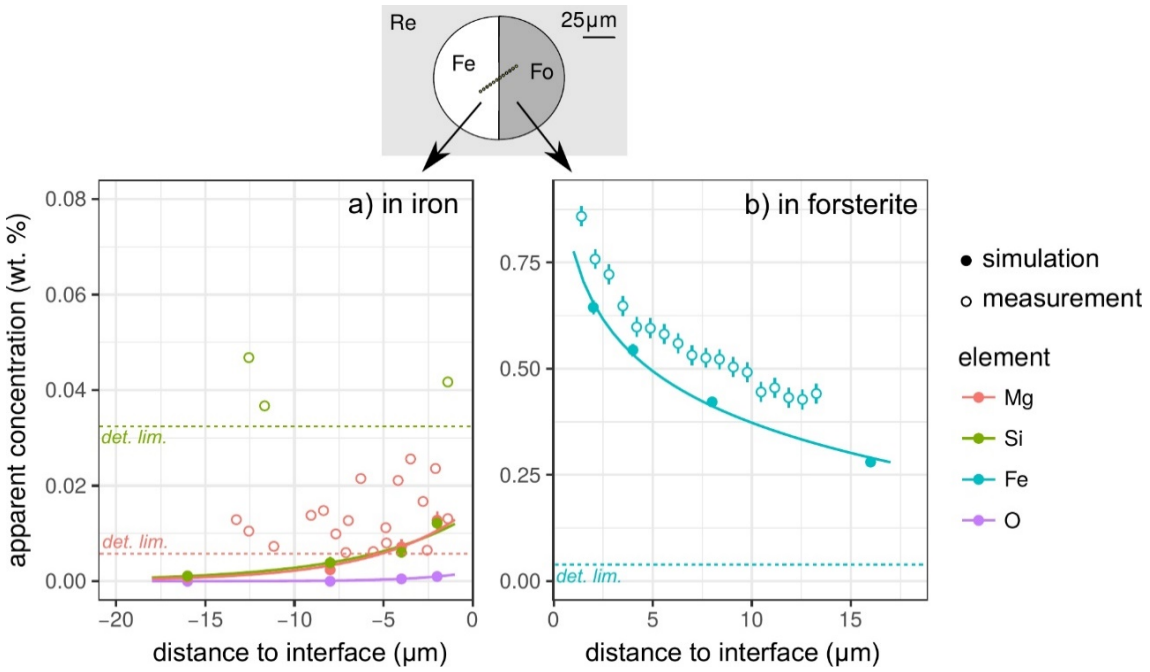

Figure 7. Simulations and EPMA measurements across a forsterite-Fe metal interface. Symbols and uncertainties as for Fig. 5. a) Apparent Si, Mg and O (simulation only) concentrations in the metal; b) apparent Fe concentrations in the forsterite. Curves are exponential fits to simulated data. Si and Mg apparent concentrations are only shown above their detection limits. Note the different y-axis scale in the two plots.

Contamination of metal analyses by spurious signal from lithophile elements is usually assumed to be negligible, given the high density of the metal and the consequent greater attenuation of soft X-rays. Wade and Wood [32] found negligible concentrations of Si and O in simulations of a 10 µm diameter metal ball in basaltic glass. Our simulations and measurements confirm this: an apparent concentration of 0.007 wt % each of Mg and Si, and less of O, would be measured in iron at a distance of 5 µm from the interface with forsterite (Fig. 7a), which is below the detection limit

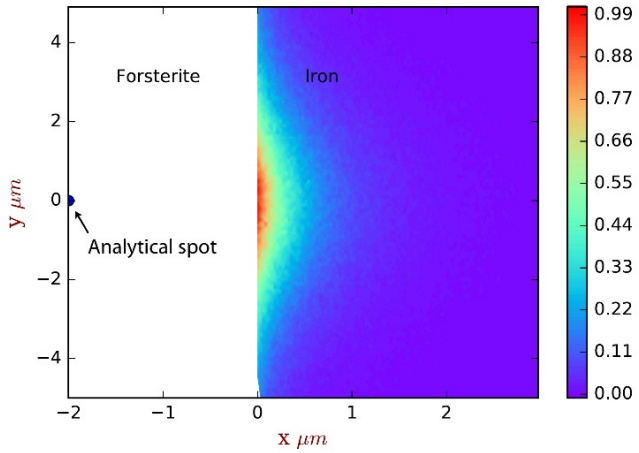

Figure 8. The spatial distribution of sites of secondary fluoresced X-ray generation projected into two dimensions, corresponding to the simulation of Figure 7. The analytical spot is in forsterite, 2 μm from the interface with iron. The colour scale is relative, showing a proportion of the maximum intensity generated.

of the EPMA measurements. The low energy O, Mg and Si $K\alpha_1$ X-rays are efficiently absorbed. However, fluorescence from the iron in measurements of the forsterite is strong: 0.6 wt% is measured 5 μm from the interface – this is well above the detection limit.

Figure 9 shows the simulated results of fluorescence arising from an iron alloy ($Fe_{15}NiCoCrMoW$) adjacent to forsterite. As well as the high fluorescence contribution from Fe, there is also a contribution from the other elements present. Figures 9a and 9b show the apparent measured concentrations: these data will typically be interpreted as oxides in a silicate phase of interest (and, as such, have a higher wt% than shown). As expected, the lowest energy lines, Mo ($L\alpha_1$) and W ($M\alpha_1$), exhibit the lowest fluorescence relative to the other minor elements. This demonstrates both the value in using lower energy lines to avoid fluorescence issues, and the advantages in performing analyses at lower accelerating voltage, where there are fewer high-energy continuum X-rays produced.

2.3.3. Secondary fluorescence and from Cu holder. DAC experiments are typically welded to Cu TEM sample holders. A very high measured apparent concentration of Cu $K\alpha_1$ (0.5 - 1.2 wt %) was detected in both wedge samples, despite them being Cu-free (Fig. 10). The apparent Cu concentrations decrease with distance but are significant even > 20 μm from the Cu holder. Measurements of metal are more affected by Cu fluorescence than silicate due to the higher continuum background resulting from the higher mean atomic number. Cu fluorescence will always problematic when micrometre-sized samples are welded to Cu holders, resulting from the relatively high energy and low attenuation of Cu ($K\alpha_1$).

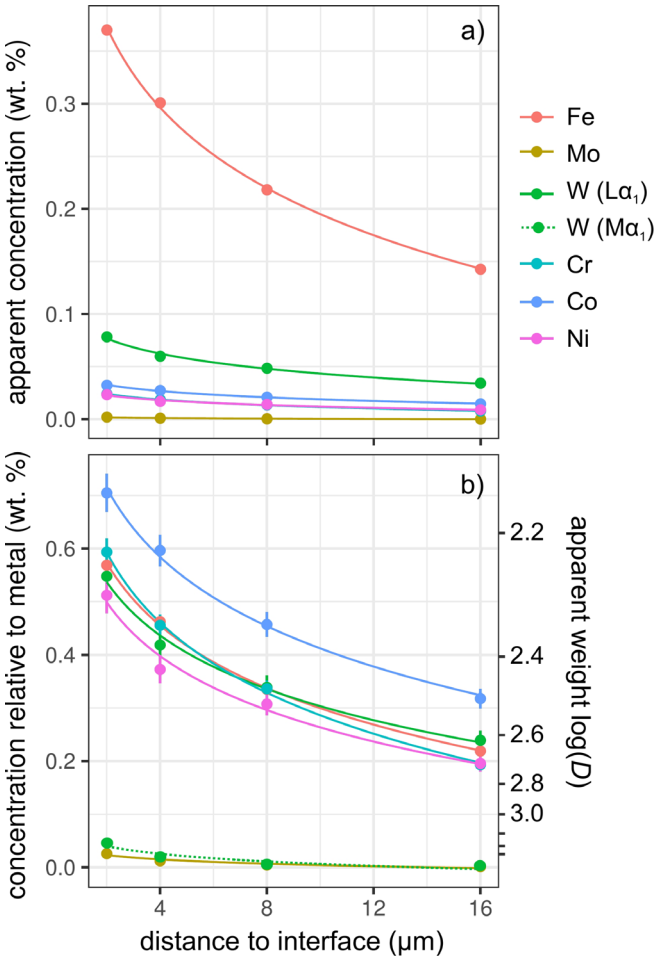

Figure 9. Simulations along a transect from a forsterite-metal ($Fe_{15}CrCoNiMoW$, mol) interface, showing points in the forsterite side only. Uncertainties and curves as in Figure 7. In (a) W-$M\alpha_1$ is hidden beneath the curve for Mo. a) Apparent concentrations in the forsterite, as a function of distance from the metal interface. b) Concentrations of the elements as a percentage of their concentrations in a $Fe_{15}CrCoNiMoW$ standard.

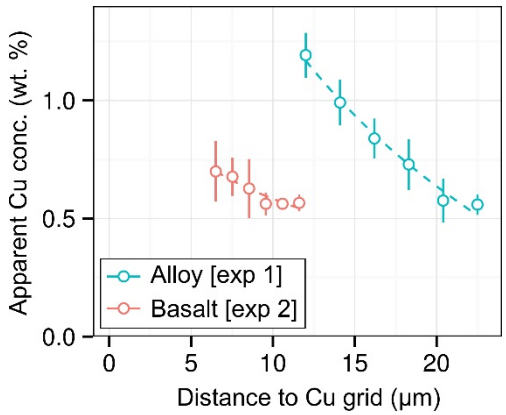

Figure 10. Open circles show apparent Cu concentrations (wt.%) from EPMA measurements of the metal wedge (blue) and the basaltic glass wedge (red). In both cases, symbols are averages of measurements equidistant from the Cu holder, and error bars are 2σ. Absolute distance to the Cu holder has a systematic error of a few μm. Dashed lines are exponential fits to the data.

2.4. Sample inhomogeneity

Sample inhomogeneity can be especially tricky in very small samples, as there may not be much room to manoeuvre to avoid these regions. For example, metal–silicate partitioning experiments performed in the DAC often display complex sub-micron scale textures in both metal and silicate phases (Fig. 12). Tiny droplets of metal are frequently present in the silicate glass and are thought to have been present during the experiment. Given the small analysable area (only ~2 - 10 μm^2) relative to the primary electron interaction volume, such metallic blebs cannot simply be avoided. The iron will be calculated as FeO, and so their accidental inclusion will result in an unexpectedly high FeO content and analytical total. Indeed, published silicate analyses from such experiments often have high totals (e.g., [6]). Inhomogeneity may also be difficult to avoid if present beneath the sample surface, or if it has a strong secondary fluorescence.

2.5. Implications for diamond anvil cell (DAC) experiments for metal-silicate partitioning: A case study for tiny samples

The conditions involved in the accretion of Earth and segregation of its core can be investigated by interpreting the depletions of various siderophile elements in its silicate crust and mantle (e.g., [38]). These depletions can be interpreted if we know how the various elements distribute themselves between molten metal and silicate, and how that partitioning behaviour changes as a function of pressure, temperature and composition. The quest to extend partitioning experiments to lower-mantle conditions has necessitated the use of laser-heated DAC experiments, where extreme pressures are reached by shrinking the sample volume to something that can be contained within a gasket between the truncated tips of two diamonds (~ 0.0001 mm^3). Usually, such experiments are run by sandwiching a small flake of iron metal foil between disks of silicate glass or compressed powder, retained within a sample chamber consisting of a narrow hole (<100 μm wide) drilled within a supporting Re gasket (Siebert *et al.* [3] describe a typical example). The experiments can be doped with a wide range of moderately siderophile elements of scientific interest (e.g., [4]), or they can be used to examine light element partitioning, such as O, Si or S, during core formation (e.g., [13, 25]). The experiments are quenched rapidly by switching off the laser, and the experimental run products invariably consist of a central metal sphere (~5 - 10 μm diameter) with a quenched silicate melt rim (~1 - 5 μm thickness), which itself is surrounded by unmelted silicate starting material (Fig. 11). Each phase tends to contain entrained or exsolved blebs of the other (Fig. 12): whether these should be avoided during analysis depends on the interpretation of their origin.

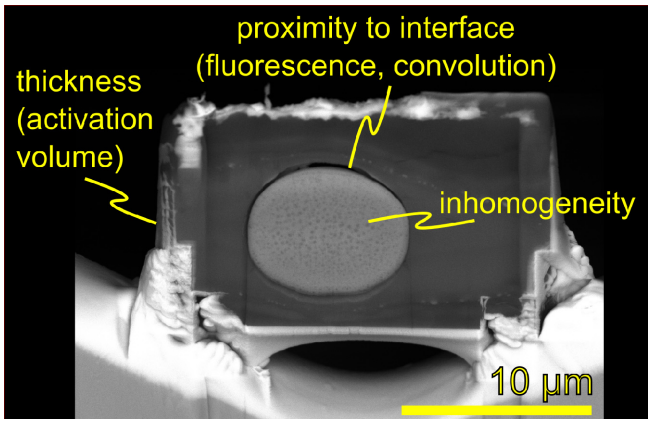

Figure 2Product of DAC metal-silicate partitioning experiment (4070 K, 37 GPa) cut by FIB for EPMA analysis.

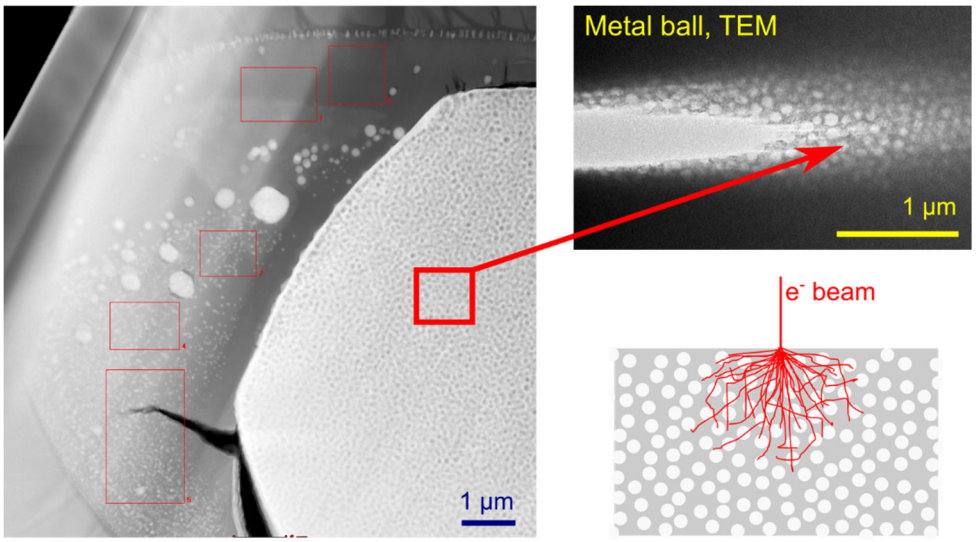

Figure 12. Left: STEM image of DAC metal-silicate partitioning experiment, prepared as a thin lamella. The phases of interest are the large metal sphere surrounded by a quenched silicate. The metal (light grey) contains uniformly-sized dark grey (oxide) heterogeneities. The silicate (dark grey) contains light grey (metal) heterogeneities of a range of sizes. Right: TEM image of the metal, showing the homogeneous size and distribution of exsolved oxide spheres. Cartoon illustrates size of exsolved spheres relative to EPMA primary electron interaction volume.

The compositions of experimental run products are typically measured by WDS by EPMA [1-4, 6, 38] or EDS [9], although other studies utilised TEM or nanoSIMS [12, 13, 25], which usually require at least major element analyses performed by EPMA based techniques if they are to yield fully quantifiable element data. The small size of DAC samples necessitates their preparation for analysis by cutting and removing a 1 - 4 µm thick slice by FIB. Typically, EPMA analyses utilise a 'standard' 15 or 20 kV_{acc} setup, with minimal consideration given to analytical artefacts which may affect the measurements of such small samples. The small sample size and

geometry presents unique analytical challenges that are especially problematic in experiments where element partitioning between coexisting chemically and physically dissimilar phases is desired [32]. An example of such an experiment, with analytical issues highlighted, is given in Fig. 11. Our recommended guidelines are:

1) *Thickness:* Electrons are less impeded by silicate, so the minimum thickness for the FIB lamella is determined by the requirements to measure the glass. We recommend 1,500 - 2,000 nm (section 2.2) at 15 kV and thicker for 20 kV. A thin film correction may be useful for a thin sample, but we do not recommend normalising to 100 % in the case of low totals from a thin sample.
2) *Fluorescence:* Fluorescence will reduce the concentration contrast between phases (section 2.3). DAC experiments are too small to mitigate by measuring further from the interface. Metal analyses should not be noticeably affected by fluorescence from light elements in the silicate. However, measurements of trace siderophile elements in the silicate are prone to significant contamination. The more strongly siderophile the element, the more difficult it will be to measure a reliable concentration ratio: an upper limit of measurable partition coefficient is suggested to be $D_{\text{met-sil}} \sim 250$. Above this, the majority of the silicate signal is an artefact of fluorescence. The problems of spurious analyses in DAC experiments are exacerbated at higher accelerating voltages, where significant continuum radiation exists above the critical excitation edge of the highest energy lines typically analysed. Using lower energy lines is a useful mitigation. Fluorescence can also be simulated and corrected for.
3) *Inhomogeneity:* This is difficult to avoid in such experiments. Using a lower kV_{acc} should help, but then other effects such as surface deposition and differences in conductive coatings become more significant. An additional analytical difficulty has been encountered when measuring the metal phase, caused by the sub-micron exsolution texture. This is discussed in section 3.1.

3. *USING APT TO INVESTIGATE NM-SCALE EXSOLUTION TEXTURES*

3.1. *Nanometre-scale heterogeneity in experimentally-quenched metals: Characterisation and consequence for EPMA measurements*

Low EPMA totals for the quenched metal phase of DAC metal-silicate partitioning experiments, combined with notoriously high O as well as high Si concentrations are frequently reported in the literature (analytical totals of < 95 % are not uncommon: [3, 4, 6, 39]). It is also a characteristic feature of published SEM and TEM images that these quenched metallic melts almost always contain densely packed and evenly dispersed sub-µm spheres, appearing as tiny dark circles on BSE images (i.e., low Z relative to Fe). In this section, we explore the nature of this sub-µm heterogeneity and its consequence for EPMA measurements.

We performed 4 new DAC partitioning experiments in a simple system (enstatite and $Fe_{91}Si_9$ starting materials), and were unable to get reasonable analytical totals (none > 92 %) by EPMA of

the metal phase of any of the samples. This was not due to the sample thickness, as the samples were 2 - 3 μm thick and the silicate totals were close to 100 %. We made measurements by both the EPMA (Bayerisches Geoinstitut) and by FEG-EPMA (University of Bristol), with and without a carbon coat, with different standards. Some of the shortfall appeared to be due to C contamination within the nominally C-free materials, although this was not able to account for the majority of the missing signal.

The metal phase in almost all cases contains a large number of ~100 nm spheres of what appears to be an immiscible, exsolved phase. These exsolved balls are near-pure SiO_2 in all cases (see below), which is probably also true in the case of most or all published experiments. These spheres present an unusual challenge: they may be causing low totals by violating the assumption of homogeneity of the $\Phi(\rho z)$ correction routine. The correction assumes that different characteristic X-rays that emerge at the surface have known depth-of-origin profiles. A second phase that is smaller than the primary analytical volume may therefore cause either high or low totals, depending on if absorption of certain X-rays are under- or over-corrected for.

Initial characterisation of these heterogeneities was done using a 5 kV_{acc} beam on a FEG-EPMA at the University of Bristol. This lower energy beam can resolve chemistry on the ~100 nm scale. Although unable to properly distinguish the exsolved features, mapping indicated a spatial correlation between Si, O, and surprisingly, C concentrations, indicating that the balls consist of SiO_2 +/- C. However, such a low kV measurement compromises the Fe measurement, as Fe-L X-rays must be used. We were again unable to produce bulk measurements of the metal with totals > ~ 92 %.

To determine if the presence of exsolved SiO_2 affects the calculation of metal compositions from EPMA measurements, we performed simulations in PENEPMA of a single isolated SiO_2 sphere embedded within a pure Fe matrix. Published analyses of metal at 15/20 kV_{acc} that appear high in Si and O can be recreated by these simulations: these oxide inclusions are too small to be reliably analysed with a beam that excites both the inclusion and the surrounding area.

3.2. APT measurement

We measured the spheres and matrix by APT in order to completely characterise both their compositions and the nature of the interface between them. Several needles from two experimental quenched metals were first prepared by FIB. These needles were prepared with thick a Pt tip to protect them from beam damage and Ga^+ implantation, which was removed in the final stages of low-energy milling. The needles were analysed at the Department of Materials, University of Oxford. Analysis was carried out using a LEAP 5000X HR at 50 K, using laser pulsing at 200 kHz with wavelength of 355 nm, pulse energy of 60 pJ and a detection rate of 0.3 %. A shank angle based reconstruction was used. There were significant multiple mass spectra overlaps between $^{24}Mg^+$,$^{24}Mg_2^{2+}$,$^{12}C_2^+$ and $^{24}MgC_2^{2+}$. Two successful analyses were obtained which included the interface between the metal matrix and the exsolved oxides (Fig. 13).

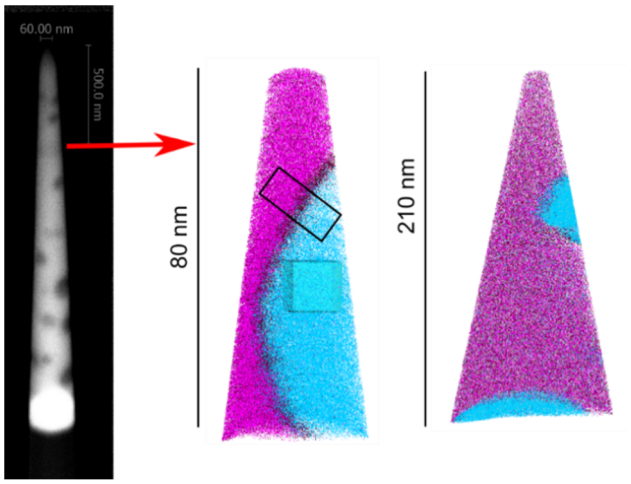

Figure 13. Left: BSE image of a needle cut by FIB for APT measurement of the metal phase. The oxide spheres and Fe-rich matrix are clearly visible. Needle is around 2 µm long from the white Pt base, and 60 nm wide just below the tip. Right: APT reconstruction of the positions and identities of the atoms in two needles from the same experiment. Fe, pink; C, maroon; O, light blue; Si, grey. Trace elements not shown. Black rectangle is position of the proxigram cylinder.

The exsolved nanospheres were found to be near-pure and near-stoichiometric SiO_2. The metal matrix was around 80 at% Fe, 12 at% C, 4 at% Si and 3 at% O. The matrix and silica spheres were remarkably homogeneous. The interface between the two was highly enriched (decorated) in C, Al, Mg, P, Cr and other trace elements that were nominally absent from the experiment. The complete compositions can be seen in Fig. 14, where each point is an integrated composition of a curved 3D slice within which points are equidistant from the interface (defined at an arbitrary Si content). This high level of compositional detail in 3D spatial geometry is only possible by APT.

3.3. Implications for partitioning experiments

The results are surprising, and have implications for the interpretation of DAC partitioning experiments. Firstly, the presence of relatively high C-concentrations in the metal matrix was unexpected given that the experiments were prepared from C-free materials, and were unknown of from EPMA measurement. It is likely that high levels of C entered the system either as laboratory contamination of the starting materials (glue, solvents, etc.), or from diffusion from the diamond surface.

Secondly, the lack of any sign of compositional gradients suggests that the growth of the exsolved silica spheres was not diffusion-limited, i.e., it is difficult to relate to polythermal quenching. It is usually considered that these spheres are quench exsolution – because Si and O are more soluble in iron at high temperature than at low temperature [13]. Because diffusion rates are extremely high, incompatible lithophile elements nucleate and diffuse out of the metal in the fraction of a second after the laser power is switched off. If this were true, one might expect compositional

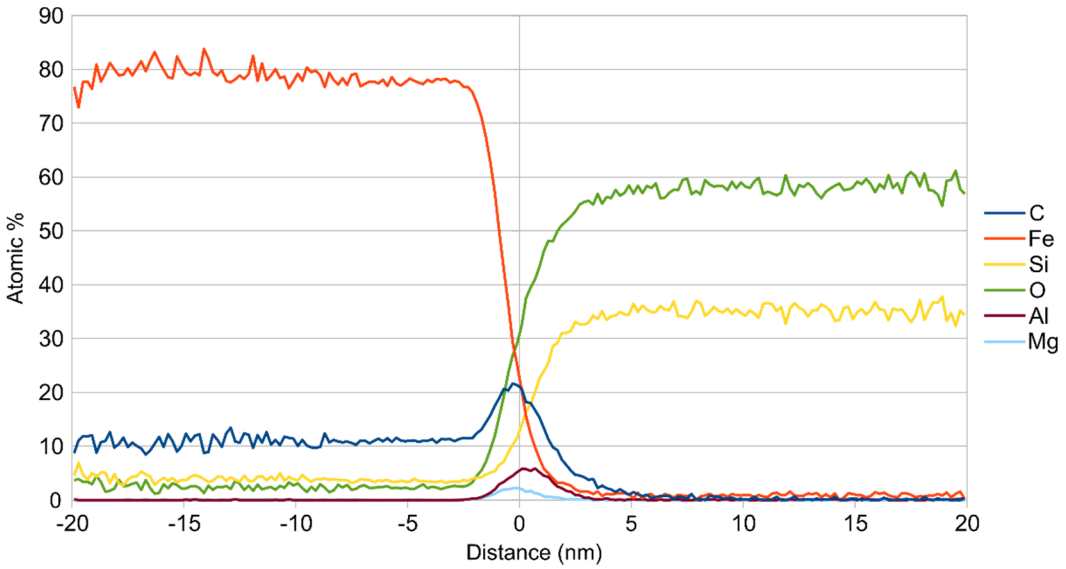

Figure 14. Proxigram (average at% concentrations) through the cylinder marked in Fig. 13. Left: BSE image of a needle cut by FIB for APT measurement of the metal phase. The oxide spheres and Fe-rich matrix are clearly visible. Needle is around 2 μm long from the white Pt base, and 60 nm wide just below the tip. Right: APT reconstruction of the positions and identities of the atoms in two needles from the same experiment. Fe, pink; C, maroon; O, light blue; Si, grey. Trace elements not shown. Black rectangle is position of the proxigram cylinder.

gradients to be frozen into the metal, as the decreasing temperature slows the diffusion and prevents further exsolution. We can speculate on alternative origins of these spheres, such as the oxidation of Si that was initially in the metal starting material. These experimental metals are usually measured by EPMA, integrating over the heterogeneous area – intrinsic to this is an assumption that the metal was a single stable phase during the experiment. However, if the spheres were stable prior to quench, then integrated metal compositions may not be relevant to equilibrium partitioning.

Finally, trace elements are concentrated at the metal–silica interface: incompatible elements are already known to accumulate at grain boundaries in order to minimise the strain energy in crystal lattices (e.g., [39]). It is unclear if the exsolution, and so the creation of grain boundaries, occurred during quench or earlier, but this observed trace element distribution has consequences for the interpretation of equilibrium trace lithophile element partitioning from such DAC experiments (e.g., [4, 38]).

The level of compositional and spatial detail presented here is of vital importance in the interpretation of DAC metal-silicate partitioning experiments, and consequently, in extrapolating from laboratory results to the formation of Earth's core. Details such as the relationship between nanostructures and host matrix would not be known without APT analysis. DAC metal-silicate partitioning experiments represent one example of a case where expanding the range of techniques used and length-scales examined has helped us to interpret tiny samples – many more varied potential cases exist.

4. CONCLUSIONS

A range of techniques are available for the quantitative analysis of chemical compositions of tiny samples (nm-to-μm length-scale). Generally, the smaller the sample and the higher precision required, the more difficult the measurement and associated sample preparation. Techniques that are appropriate for measuring the compositions of tiny samples include, but are not limited to, those that rely on the generation and measurement of characteristic X-rays (EPMA, SEM, TEM, μXRF) as well as secondary ions (nanoSIMS and ATP).

EPMA remains the most popular and commonly-used technique for samples down to several μm, due to its convenience (ease of sample preparation and calibration) and relatively high sensitivity. However, users must be cautions when the length-scales being measured approach the size of the primary interaction volume. As samples become thin, electrons and photons can be lost through the base, reducing X-ray production relative to thick standards. Given that measured characteristic X-rays will have different energy-dependent profiles of depth of origin, this can affect elements to different extents. When measuring close to grain boundaries, similar issues exist. If the primary interaction volume cuts across an interface, then primary X-rays will be generated from the wrong phase. However, even at distances of ten of μm from an interface, a significant signal can be generated from secondary fluoresced X-rays, given that X-rays are less impeded than electrons. Such spurious signals are problematic when measuring trace concentrations in close proximity to major concentrations [32] or when measuring diffusion gradients across interfaces for geothermometry/speedometry purposes [35]. In general, interaction volumes and distances from which secondary X-rays can be fluoresced are smaller at lower kV_{acc} and for denser materials such as metals. Fluorescence will be exacerbated by the presence of small heterogeneities – by metal globules entrained in the quenched silicate, and vice-versa.

We consider these limitations in the case of DAC metal-silicate partitioning experiments, where analyses are both a) of thin samples and b) close to interfaces where strong compositional contrasts exist, and provide recommendations for EPMA analyses in section 2.5.

Monte Carlo simulations are an effective way to explore these data artefacts, and as with previous studies, we have found them to reliably reproduce real EPMA analyses. We recommend that, when working with small or difficult samples, simulations are used to check the integrity of the measurement.

One additional difficulty was found in EPMA measurements when sub-μm heterogeneities were present. As a case study, we have presented a study on exsolution textures in quenched DAC metal-silicate partitioning experiments. Such experiments are routinely analysed by EPMA, using a relatively large spot to integrate the composition of exsolved phases and the host matrix. However, poor analytical totals are a common feature of the metal phase: this may be a fundamental problem with quantifying light element concentrations when an exsolution texture is present. The

exsolved phase was examined by APT. It was found to be pure silica, with a lack of any compositional gradients in the matrix metal and a trace-element-enriched interface. This requires a reconsideration of the origin of this texture as a quench feature, presenting the possibility that the silica spheres were present at experimental high temperature, and thus are not interpreted as belonging to the equilibrium metal composition.

5. REFERENCES

[1] Bouhifd M A and Jephcoat A P 2003 The effect of pressure on partitioning of Ni and Co between silicate and iron-rich metal liquids: a diamond-anvil cell study. *Earth Planet. Sci. Lett.* **209** 245-255

[2] Bouhifd M A and Jephcoat A P 2011 Convergence of Ni and Co metal–silicate partition coefficients in the deep magma-ocean and coupled silicon–oxygen solubility in iron melts at high pressures. *Earth Planet. Sci. Lett.* **307** 341-348

[3] Siebert J, Badro J, Antonangeli D and Ryerson F J 2012 Metal–silicate partitioning of Ni and Co in a deep magma ocean. *Earth Planet. Sci. Lett.* **321-322** 189-197

[4] Blanchard I, Siebert J, Borensztajn S and Badro J 2017 The solubility of heat-producing elements in Earth's core. *Geochem. Perspect. Lett.* **5** 1-5

[5] Siebert J., *et al.* 2018 Chondritic Mn/Na ratio and limited post-nebular volatile loss of the Earth. *Earth Planet. Sci. Lett.* **485** 130-139

[6] Mahan B, *et al.* 2018 Constraining compositional proxies for Earth's accretion and core formation through high pressure and high temperature Zn and S metal-silicate partitioning. *Geochim. Cosmochim. Acta*. **235** 21-40

[7] Tateno S, Hirose K and Ohishi Y 2014 Melting experiments on peridotite to lowermost mantle conditions. *J. Geophys. Res. Solid Earth* **119** 4684-4694

[8.] Sinmyo R and Hirose K 2010 The Soret diffusion in laser-heated diamond-anvil cell. *Phys. Earth Planet. Inter.* **180** 172-178

[9] Chidester B A, Rahman Z, Righter K and Campbell A J 2017 Metal–silicate partitioning of U: Implications for the heat budget of the core and evidence for reduced U in the mantle. *Geochim. Cosmochim. Acta*. **199** 1-12

[10] Miyajima N, *et al.* 2010 Combining FIB milling and conventional Argon ion milling techniques to prepare high-quality site-specific TEM samples for quantitative EELS analysis of oxygen in molten iron. *J. Microscopy* **238** 200-209

[11] Wirth R 2009 Focused ion beam (FIB) combined with SEM and TEM: Advanced analytical tools for studies of chemical composition, microstructure and crystal structure in geomaterials on a nanometre scale. *Chem. Geol.* **261** 217-229

[12] Frost D J, *et al.* 2010 Partitioning of oxygen between the Earth's mantle and core. *J. Geophys. Res. Solid Earth* **115** B02202

[13] Fischer R A, *et al.* 2015 High pressure metal–silicate partitioning of Ni, Co, V, Cr, Si, and O. *Geochim. Cosmochim. Acta* **167** 177-194

[14] Schmidt C and Rickers K 2003 In-situ determination of mineral solubilities in fluids using a hydrothermal diamond-anvil cell and SR-XRF: Solubility of AgCl in water. *Am. Mineralogist* **88** 288-292
[15] Petitgirard S, *et al.* 2009 A diamond anvil cell for x-ray fluorescence measurements of trace elements in fluids at high pressure and high temperature. *Rev. Sci. Instrum.* **80** 033906
[16] Manning C E, Wilke M, Schmidt C and Cauzid J 2008 Rutile solubility in albite-H2O and Na2Si3O7-H2O at high temperatures and pressures by in-situ synchrotron radiation micro-XRF. *Earth Planet. Sci. Lett.* **272** 730-737
[17] Andrault D, *et al.* 2012 Solid–liquid iron partitioning in Earth's deep mantle. *Nature* **487** 354-357
[18] Petitgirard S, *et al.* 2012 An in situ approach to study trace element partitioning in the laser heated diamond anvil cell. *Rev. Sci. Instrum.* **83** 013904
[19] Gault B, Moody M P, Cairney J M and Ringer S P 2012 *Atom probe microscopy.* (New York, NY: Springer Science & Business Media)
[20] Valley J W, *et al.* 2014 Hadean age for a post-magma-ocean zircon confirmed by atom-probe tomography. *Nature Geosci.* **7** 219-223
[21] White L F, *et al.* 2017 Atomic-scale age resolution of planetary events. *Nature Commun.* **8** 15597
[22] Lewis J B, Isheim D, Floss C and Seidman D N 2015 C12/C13-ratio determination in nanodiamonds by atom-probe tomography. *Ultramicroscopy* **159** 248-254
[23] Zinner E 2007 in: *Treatise on geochemistry.* (Holland H D and Turekian K K; Eds.) (Oxford, UK: Pergamon) 1-33
[24] Badro J, *et al.* 2007 Chemical imaging with NanoSIMS: A window into deep-Earth geochemistry. *Earth Planet. Sci. Lett.* **262** 543-551
[25] Suer T-A, Siebert J, Remusat L, Menguy N and Fiquet G 2017 A sulfur-poor terrestrial core inferred from metal–silicate partitioning experiments. *Earth Planet. Sci. Lett.* **469** 84-97
[26] Pouchou J-L and Pichoir F 1991 in: *Electron probe quantitation.* (Boston, MA: Springer) 31-75
[27] Love G, Cox M G and Scott V D 1978 A versatile atomic number correction for electron-probe microanalysis. *J. Phys. Appl. Phys.* **11** 7
[28] Armstrong J T 1991 in: *Electron probe quantitation.* (Boston, MA: Springer) 261-315
[29] Acosta E, Llovet X, Coleoni E, Riveros J A and Salvat F 1998 Monte Carlo simulation of x-ray emission by kilovolt electron bombardment. *J. Appl. Phys.* **83** 6038-6049
[30] Llovet X and Salvat F 2017 PENEPMA: A Monte Carlo program for the simulation of X-ray emission in electron probe microanalysis. *Microsc. Microanal.* **23** 1-13
[31] Salvat F, Fernández-Varea J M and Sempau J 2008 in: *Workshop Proceedings* (Barcelona, Spain: OECD) NEA No. 6416.
[32] Wade J and Wood B J 2012 Metal–silicate partitioning experiments in the diamond anvil cell: A comment on potential analytical errors. *Phys. Earth Planet. Inter.* **192-193** 54-58
[33] Armstrong J T 1995 CITZAF: a package of correction programs for the quantitative electron microbeam X-ray analysis of thick polished materials, thin-films, and particles. *Microbeam Anal.* **4** 177-200

[34] Green M 1964 The angular distribution of characteristic x radiation and its origin within a solid target. *Proc. Phys. Soc.* **83** 435
[35] Borisova A Y, *et al.* 2018 Secondary fluorescence effects in microbeam analysis and their impacts on geospeedometry and geothermometry. *Chem. Geol.* **490** 22-29
[36] Dalton J A and Lane S J 1996 Electron microprobe analysis of Ca in olivine close to grain boundaries; the problem of secondary X-ray fluorescence. *Amer. Mineralogist* **81** 194-201
[37] Walter M J, Newsom H E, Ertel W and Holzheid A 2000 in: *Origin of the Earth and Moon.* (Tucson, AZ: University of Arizona Press) 265-289
[38] Badro J, Siebert J and Nimmo F 2016 An early geodynamo driven by exsolution of mantle components from Earth's core. *Nature* **536** 326-328
[39] Hiraga T, Anderson I M and Kohlstedt D L 2004 Grain boundaries as reservoirs of incompatible elements in the Earth's mantle. *Nature* **427** 699-703